Determination of the Conformation of 2-Hydroxy- and 2-Aminobenzoic Acid Dimers Using ^{13}C NMR and Density Functional Theory/Natural Bond Order Analysis: The Central Importance of the Carboxylic Acid Carbon

Ronald R. Burnette* and Frank Weinhold

School of Pharmacy and the Department of Chemistry, University of Wisconsin, Madison, Wisconsin 53705

Received: November 30, 2005

The ^{13}C chemical shift for the carboxylic acid carbon provides a powerful diagnostic probe to determine the preferred isomeric dimer structures of benzoic acid derivatives undergoing intra- and intermolecular H-bonding in the gas, solution and crystalline phases. We have employed hybrid density functional calculations and natural bond orbital analysis to elucidate the electronic origins of the observed ^{13}C shieldings and their relationship to isomeric stability. We find that delocalizing interactions from the carbonyl oxygen lone pairs (n_O) into vicinal carbon−oxygen and carbon−carbon antibonds (σ^*_{CO},σ^*_{CC}) make critical contributions to the ^{13}C shieldings, and these $n_O \rightarrow \sigma^*_{CO}$, $n_O \rightarrow \sigma^*_{CC}$ interactions are in turn sensitive to the intramolecular interactions that dictate dimer structure and stability. The carboxyl carbon atom can thus serve as a useful detector of subtle structural and conformational features in this pharmacologically important class of carboxylic acid interactions.

Introduction

It has been pointed out that the accurate calculation of ^{13}C chemical shifts could become a method which complements ^{1}H−^{1}H coupling constants, ^{1}H−^{1}H NOE measurements, and empirical chemical shift correlations for the determination of the configurations of organic molecules.[1] In the interest of computational economy, it then becomes of particular concern to determine the validity of using gas phase calculations to predict chemical shifts for molecules in solution. At present the most common NMR solvent used for organic molecules is probably $CDCl_3$.[2] In addition, chloroform has recently been shown to be a good model for the center of a lipid bilayer and as such conformational studies in chloroform may well be applicable to that obtained in the lipid bilyer.[3,4] The question of the importance of solvent effect can be approached by comparing gas phase chemical shift calculations with experimentally determined ^{13}C chemical shifts in $CDCl_3$. Previous investigations have demonstrated the feasibility of obtaining calculated ^{13}C chemical shifts that are within 1−2 ppm of the experimental ^{13}C chemical shifts.[1,5] This high degree of agreement occurs when the appropriate model chemistry is used[5] and if empirical scaling between theoretical isotropic shielding and experimental ^{13}C chemical shifts is applied through the use of a calibration curve obtained from a structurally related reference molecule(s).[1,6] However, this demonstration by itself may be inadequate, because one must also be able to find useful model systems that are within available computer resources. Thus, the ability to efficiently obtain results of appropriate computational accuracy is essential, and studies have shown that the use of less complex model molecules can be used to one's advantage in this regard.[7]

A related question regarding the calculation of chemical shifts is: How transferable are these results to other molecules having similar functional groups? If the primary contributions to the chemical shift are localized to nearest neighbors, then one could infer that the transferability of these results to similar molecules might be feasible. Empirical correlations between observed chemical shift and summation of functional group shifts indeed suggest this to be the case.[8] One method by which these empirical correlations can be interpreted from a more fundamental point of view is to use natural chemical shift analysis (NCS),[9] a localized analysis of NMR shielding within the natural bond orbital (NBO) framework. Within the G98[10]-based GIAO (gauge-including atomic orbitals)[11,12] framework, NCS gives an NBO/NLMO (natural bond orbital/natural localized molecular orbital) based analysis of unperturbed (field-free) and induced (field-dependent) contributions to NMR chemical shielding tensors. As such, NCS analysis allows one to decompose the observed chemical shifts into component contributions from localized σ-bonds, π-bonds, lone pair and the associated non-Lewis delocalization effects between the different atoms present in the molecule. Such decomposition facilitates understanding of how ^{13}C chemical shifts reflect local and nonlocal features of molecular structure.

To explore these issues further, we have investigated 2-hydroxybenzoic acid (2HBA) and 2-aminobenzoic acid (2ABA) in $CDCl_3$ at 298 K. Along with the experimental measurement of the ^{13}C chemical shifts, NBO analyses were carried out to characterize the optimized structures, their stabilities, and the ^{13}C chemical shifts.[13] This system of molecules allows for the assessment of long-range resonance effects, intramolecular hydrogen bonding, intermolecular hydrogen bonding, the interplay between simultaneous intermolecular and intramolecular hydrogen bonding interactions, and lone pair electron contributions from oxygen and nitrogen on ^{13}C chemical shift decomposition, its transferability and relationship to molecular structure. In addition, because extensive X-ray crystallographic data are available for these molecules, the study allows comparisons between gas phase calculated structures and those found in the crystalline state. Carbon-13 chemical shifts have been chosen

* Corresponding author. E-mail: rrburnette@pharmacy.wisc.edu.

10.1021/jp058300w CCC: $33.50
Published on Web 06/22/2006

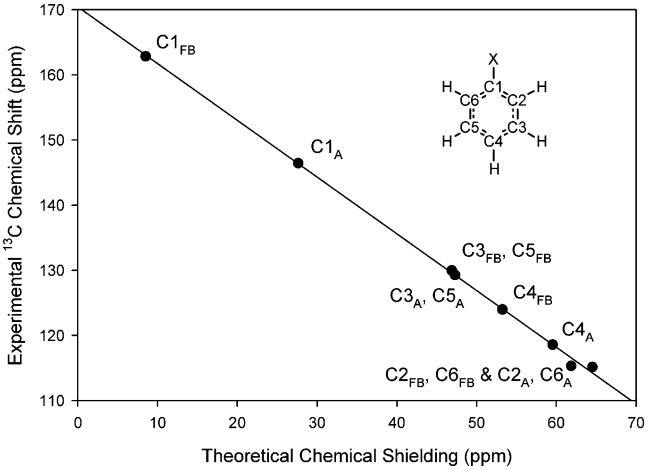

Figure 1. Calibration curve for conversion between isotropic ^{13}C chemical shielding and experimental ^{13}C chemical shifts (relative to TMS) for 100 mM fluorobenzene and aniline in $CDCl_3$ at 298 K. The fitted line is $y = 170.45 - 0.8710x$ with $r^2 = 0.998$, where y is the ^{13}C experimental chemical shift in ppm and x is the calculated ^{13}C isotropic magnetic shielding, obtained in GIAO framework using a B3LYP/6-311+G(2d,p) model chemistry based on optimized B3LYP/6-31+G-(d) geometry. The individual ^{13}C chemical shifts for each carbon are indicated on the figure as C1−C6 (see inset figure of the molecule for the numbering scheme) where X is F or NH_2 and is FB for fluorobenzene and A for aniline.

over proton chemical shifts for study because of the 10-fold greater chemical range afforded by ^{13}C spectra and because the ^{13}C backbone structure is somewhat shielded from solvent molecules by the covalently bonded protons.

Methods

Experimental ^{13}C chemical shifts were obtained using standard Bruker pulse sequences on a 500 MHz NMR spectrometer. Structural assignments were accomplished through the use of 1-D ^{1}H, ^{13}C, and 2-D ^{1}H−^{13}C HETCOR and ^{1}H NOESY experiments.[14] Spectra were obtained for 100 mM fluorobenzene, aniline, 2HBA and 2ABA in $CDCl_3$ at 298 K with tetramethylsilane (TMS) as an internal reference for ^{1}H and ^{13}C spectra. Figure 1 is the calibration curve obtained from fluorobenzene and aniline. The linear fit has an r^2 of 0.998 for the regression equation $y = 170.45 - 0.8710x$ ppm, where y is the experimental ^{13}C chemical shift (referenced to TMS) and x is the calculated isotropic ^{13}C chemical shielding. In the present work, the linear regression equation obtained from Figure 1 was used to determine the calculated ^{13}C chemical shifts. Fluorobenzene and aniline were chosen for the calibration curve because they have a ^{13}C chemical shift range similar to that of the benzoic acids and yet do not contain a carboxylic acid carbon. This avoids the cyclic dimerization typically observed with benzoic acids in chloroform.[15]

Figure 2 shows the chemical structures and numbering scheme used in all calculations and discussions. Figure 3 gives the possible generic rotamers and associated isomers of the dimer benzoic acid derivatives considered in this work.

Initial lowest energy starting conformations were obtained through the use of MMFF molecular mechanic conformational searches using Titan.[16] Subsequently, final monomer and model dimer conformer optimization was determined by obtaining B3LYP/6-31+G(d) optimized geometries using Gaussian 98[10] (G98). Vibrational frequency analysis revealed no imaginary frequencies, indicating that the final structures correspond to true minima on the potential energy surface. These optimized

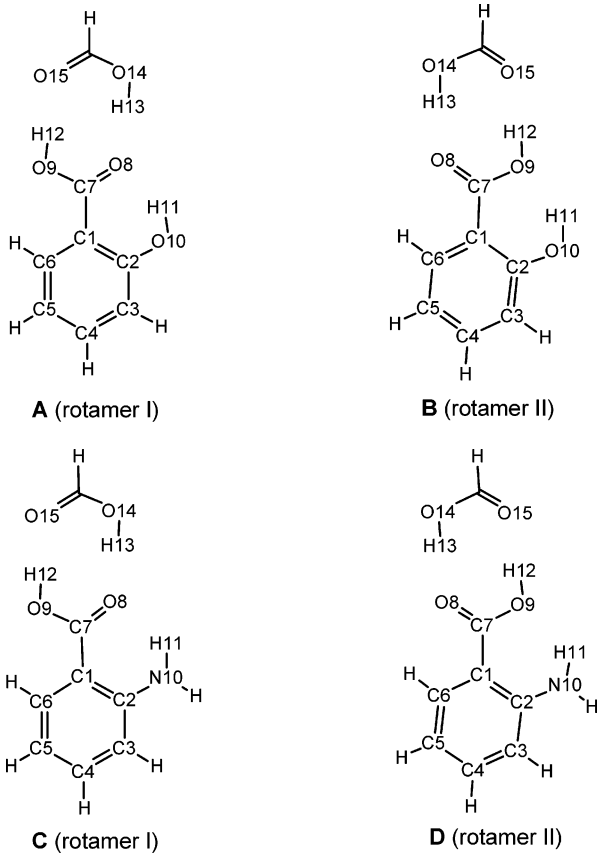

Figure 2. Chemical structural dimer model of benzoic acid derivatives and formic acid used in all calculations. (A) is the 2HBA/formic acid dimer rotamer I, and (B) is the 2HBA/formic acid dimer rotamer II; (C) is the 2ABA/formic acid dimer rotamer I, and (D) is the 2ABA/formic acid dimer rotamer II.

geometries were then used in subsequent natural bond orbital analyses and in the determination of higher level single point energies and NMR shieldings, carried out using a B3LYP/6-311+G(2d,p)[5] treatment. The calculated shieldings were then subjected to NCS analysis[8] to obtain the isotropic ^{13}C shielding tensors and their decomposition into component parts. Second-order perturbative estimates of donor−acceptor (bond-antibond) interactions in the NBO basis were obtained by standard NBO analysis.[13] The natural charges residing on the individual atoms were obtained from a natural population analysis (NPA) and bond orders were obtained by using natural resonance theory (NRT),[13] all standard options of the NBO 5.0[17] program interfaced to G98. Orbital graphics were accomplished through the use of NBOView 1.0.[18] In addition, dimer optimizations were carried out at B3LYP/6-31G. Frequency analysis at B3LYP/6-31G revealed no imaginary frequencies and SCF single point energies were determined from these optimized structures at B3LYP/6-31+G(d). All calculations were done on a 1.8 GHz 50 processor Linux cluster having 1 GB of RAM available per processor.

Results and Discussion

Table 1 summarizes and compares the calculated ^{13}C chemical shifts to the experimental ^{13}C chemical shifts for the two primary rotamers of the 2HBA and 2ABA monomers. Table 2 provides a similar summary and comparison for the 2HBA and 2ABA model dimers. From Tables 1 and 2, it is clear that substantial improvement is obtained for the calculated carboxylic acid carbon (C7) ^{13}C shift when one goes from the monomer to the

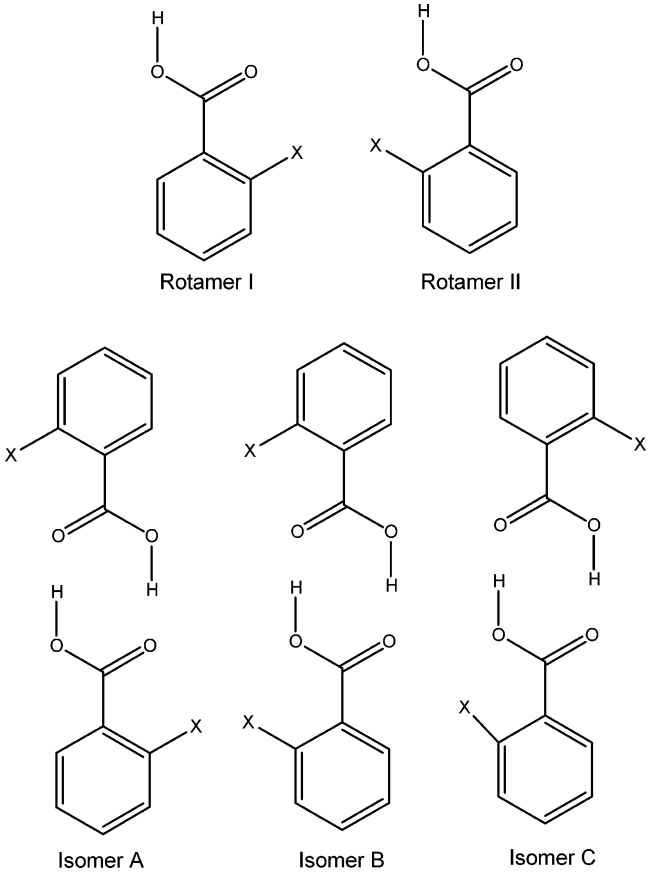

Figure 3. Generic substituted benzoic acid rotamers and the various possible isomers. X refers to either −OH or $-NH_2$. Isomer A (100% rotamer I), Isomer B (50% rotamer I and 50% rotamer II) and Isomer C (100% rotamer II).

dimer, indicative of strong intermolecular interaction effects on the carbon shielding. The calculated ^{13}C shifts of the other carbons are typically within 1−2 ppm of the experimental values and therefore are not subject to further analysis because current computation techniques are limited to this range of accuracy.[1,5]

It is known that complexation of the benzoic acid derivatives can occur and that this is primarily due to a cyclic dimerization of the carboxylic acid moieties. This is supported by numerous experimental observations showing that carboxylic acids form cyclic dimers in some organic solvents and in the vapor phase.[19] In particular, experiments by Wall[20] demonstrate that benzoic acid forms dimers in the nonpolar solvent benzene. Given that chloroform is a relatively nonpolar solvent that is freely miscible in benzene, a similar dimer-forming behavior might be anticipated for the benzoic acids in chloroform. In fact, the dimerization constant of benzoic acid is reported to have a mean value of 202 M^{-1} in benzene and 192 M^{-1} in chloroform using the distribution method.[15] Also, at saturable concentrations of benzoic acid or 2-fluorobenzoic acid, even in the polar solvent water, dimer formation has been observed using conductance measurements as the experimental probe.[21]

NBO analysis of the intermolecular interaction suggests how we can further simplify the computational model. The intermolecular H-bonding interactions between monomers are found to arise from two strong NBO donor−acceptor interactions (of typical $n_O \rightarrow \sigma^*_{OH}$ type, cooperatively enhanced by their complementary directionality) that are well localized on the carbonyl groups. The electronic shielding properties of a particular monomer are therefore primarily sensitive to the *presence* of the second carboxyl group, rather than to the details of its

TABLE 1: Experimental and Calculated ^{13}C Spectral Shifts for Monomers[a]

carbon no.	exp (ppm)	2-HBA rotamer I (Figure 2A) theory[b]	cal (ppm)[b]	|dif|	2-HBA rotamer II (Figure 2B) theory[b]	cal (ppm)[b]	|dif|
1	111.3	67.5	111.7	0.4	65.9	113.1	1.8
2	162.2	9.3	162.4	0.2	13.4	158.8	3.4
3	117.9	59.5	118.7	0.8	59.5	118.6	0.7
4	137.0	39.4	136.1	0.9	39.8	135.8	1.2
5	119.6	59.5	118.7	1.0	58.0	119.9	0.3
6	131.0	45.4	130.9	0.1	41.9	133.9	2.9
7	**174.9**	**3.5**	**167.4**	**7.5**	**10.6**	**161.2**	**13.7**

carbon no.	exp (ppm)	2-ABA rotamer I (Figure 2C) theory[b]	cal (ppm)[b]	|dif|	2-ABA rotamer II (Figure 2D) theory[b]	cal (ppm)[b]	|dif|
1	109.6	70.0	109.5	0.1	67.3	111.8	2.2
2	151.1	23.6	149.9	1.2	25.9	147.9	3.3
3	116.5	63.4	115.2	1.3	62.6	115.9	0.6
4	135.1	41.3	134.5	0.6	41.2	134.5	0.6
5	116.8	62.9	115.7	1.1	61.0	117.3	0.5
6	132.2	43.3	132.8	0.6	40.2	135.4	3.2
7	**173.6**	**5.9**	**165.3**	**8.3**	**9.0**	**162.6**	**11.0**

[a] Experimental and calculated ^{13}C chemical shifts along with absolute difference (|dif|) errors for the two principal monomer rotamers of 2-hydroxybenzioic acid (2-HBA) and 2-aminobenzoic acid (2-ABA). The most significant differences occur with the carboxylic acid carbon (C7) and are indicated by bold print. [b] The theory column contains the ab initio NMR shielding values which, when applied to the regression relation obtained from Figure 1, allows for the determination of the values given in the cal column.

TABLE 2: Experimental and Calculated ^{13}C Spectral Shifts for Dimers[a]

carbon no.	exp (ppm)	2-HBA/FA rotamer I (Figure 2A) theory[b]	cal (ppm)[b]	|dif|	2-HBA/FA rotamer II (Figure 2B) theory[b]	cal (ppm)[b]	|dif|
1	111.3	66.5	112.6	1.3	65.5	113.4	2.1
2	162.2	9.5	162.2	0.1	12.1	160.0	2.3
3	117.9	59.5	118.6	0.7	59.3	118.8	0.9
4	137.0	39.0	136.5	0.5	39.4	136.1	0.9
5	119.6	59.1	119.0	0.6	58.6	119.5	0.2
6	131.0	44.5	131.7	0.8	42.5	133.4	2.5
7	**174.9**	**−2.7**	**172.8**	**2.1**	**2.1**	**168.6**	**6.3**

carbon no.	exp (ppm)	2-ABA/FA rotamer I (Figure 2C) theory[b]	cal (ppm)[b]	|dif|	2-ABA/FA rotamer II (Figure 2D) theory[b]	cal (ppm)[b]	|dif|
1	109.6	69.1	110.3	0.7	67.5	111.6	2.1
2	151.1	23.8	149.7	1.4	25.1	148.6	2.5
3	116.5	63.3	115.4	1.1	62.4	116.1	0.4
4	135.1	40.6	135.1	0.1	40.8	134.9	0.2
5	116.8	62.4	116.1	0.7	61.8	116.6	0.2
6	132.2	42.5	133.4	1.3	40.8	134.9	2.7
7	**173.6**	**−0.9**	**171.2**	**2.4**	**1.2**	**169.4**	**4.2**

[a] Experimental and calculated ^{13}C chemical shifts along with absolute difference (|dif|) errors for the model dimers of 2-hydroxybenzioic acid (2-HBA) and 2-aminobenzoic acid (2-ABA) with formic acid (FA). The most significant differences occur with the carboxylic acid carbon (C7) and are indicated by bold print. [b] The theory column contains the ab initio NMR shielding values which, when applied to the regression relation obtained from Figure 1, allows for the determination of the values given in the cal column.

electronic environment. This implies that shielding properties of a given monomer may be adequately modeled by replacing the second monomer by the simplest possible carboxylic acid (i.e., formic acid) for computational economy. Thus, the bulk of our calculations were performed with mixed benzoic/formic acid cyclic dimers, which were found to satisfactorily emulate

the behavior of the full benzoic acid dimers, with considerable computational savings.

Use of simple carboxylic acid dimers as a computational model should not suggest that gaseous, liquid, and crystalline phases are assumed to consist only of such cyclic dimers. Indeed, it is quite likely that chainlike or other higher-order complexes may be present in particular phases. However, the key feature for each monomer is that its carboxyl group participates in *two* strong complementary H-bonding interactions, and it is only of secondary importance whether these H-bonds involve a single monomer (as in our model) or a more extended chain- or ring-like network. Thus, we believe that our simplified dimer model adequately captures the essential features of intermolecular interaction that are necessary to obtain agreement with experimental ^{13}C shielding values at a meaningful level.

Examination of Tables 1 and 2 reveals that rotamer I is favored over rotamer II for both the 2HBA and 2ABA monomers and model dimers as assessed by improved agreement of C7 ^{13}C chemical shifts. This same trend is also observed if the calculated SCF (self-consistent-field) relative energies are considered. That is, the 2HBA rotamer I monomer is 4.0 kcal/mol more stable than the 2HBA rotamer II monomer and the 2HBA rotamer I model dimer is 2.4 kcal/mol more stable than the 2HBA rotamer II model dimer. Likewise the 2ABA rotamer I monomer is 3.2 kcal/mol more stable than the 2ABA rotamer II monomer and the 2ABA rotamer I model dimer is 1.7 kcal/mol more stable than the 2ABA rotamer II model dimer. Similar results are obtained if the calculated relative free energies at 298 K are compared. This suggests that calculated ^{13}C chemical shifts that are in closest agreement with experiment are indeed consistent with the lowest energy conformation.

Improvement in the correlation between the observed experimental ^{13}C chemical shifts and theory was attempted by using a Boltzmann weighted average of the calculated ^{13}C chemical shifts for rotamers I and II. This resulted in no further improvement over that obtained from just using the lower energy rotamer's calculated ^{13}C chemical shifts. As such, only the lowest energy monomers and model dimer rotamers will be used in subsequent analysis.

Analysis of the natural charges, bond order, and bond lengths demonstrates that the cyclic dimer hydrogen bonds exhibit resonance assisted stabilization.[22,23] That is, when averaged over both rotamers of 2HBA and 2ABA, the carbonyl C7−O8 bond order is decreased (−0.052 ±0.009) with a corresponding increase (+0.0200 ± 0.0003 Å) in C7−O8 bond length, the hydroxyl C7−O9 bond order is increased (+0.042 ± 0.004) with a corresponding decrease (−0.031 ± 0.002 Å) in C7−O9 bond length, the natural charge on the carbonyl oxygen (O8) becomes more negative (−0.071 ± 0.003) and the hydroxyl oxygen (O9) becomes more positive (+0.005 ± 0.001). (See Supporting Information for detail.)

The stabilization energy analyses using second-order perturbation theory of the two rotamers of 2HBA and 2ABA are given in Tables 3−6, for the model dimers (Tables 3 and 5) and monomers (Tables 4 and 6). Overlap contour plots for representative orbital interaction entries of Tables 3−6 are provided in Figures 5−7.

Examination of Tables 3−6 reveals that the principal orbital interaction leading to the preference of one rotamer over another is dictated by the following trends. Both for the model dimers and for the monomers the primary reason for rotamer I being favored is an increased stabilization of 10.54 kcal/mol for the 2HBA dimer and 9.00 kcal/mol for the 2HBA monomer (5.52 kcal/mol for the 2ABA dimer and 12.76 kcal/mol for the 2ABA monomer), resulting from the $n''_{O9} \rightarrow \pi^*_{C7O8}$ interaction. This increased stabilization is due both to a decrease in the energy difference between the orbitals and to an increase in the extent of orbital overlap. For 2HBA and 2ABA, this stabilizing effect on the preferred conformation is partially offset by a destabilizing $n''_{O8} \rightarrow \sigma^*_{C1C7}$ interaction equaling 4.07 kcal/mol for the 2HBA dimer and 4.13 kcal/mol for the 2HBA monomer (3.42 kcal/mol for the 2ABA dimer and 5.25 kcal/mol for the 2ABA monomer). In addition, for rotamer I of 2ABA, both the model dimer and the monomer exhibit an additional stabilization resulting from the $n_{N10} \rightarrow \pi^*_{C1C2}$ interaction (6.82 kcal/mol for the 2ABA dimer and 10.31 kcal/mol for the 2ABA monomer), a consequence of both a decrease in energy difference and an increase in orbital overlap. Also, but for only the monomer of 2HBA, there is a further stabilization of rotamer I equal to 3.02 kcal/mol for the $n''_{O10} \rightarrow \pi^*_{C1C2}$ interaction, resulting principally from an increase in orbital overlap.

Intramolecular hydrogen bonding contributes to the preference of rotamer I over rotamer II for both the monomers and model dimers of 2HBA and 2ABA. In all cases, the reason for the increased rotamer I stabilization is because of an additional $n'_{O8} \rightarrow \sigma^*_{O10H11}$ interaction for 2HBA and both $n'_{O8} \rightarrow \sigma^*_{N10H11}$ and $n''_{O8} \rightarrow \sigma^*_{N10H11}$ interactions for 2ABA, which are not

TABLE 3: Primary Energy of Stabilization Interactions for 2HBA Model Dimer[a]

interaction type[b]	donor NBO (i) to acceptor NBO (j)	$E(2)$, kcal/mol rotamer I	$E(2)$, kcal/mol rotamer II	$E(2)$ difference, kcal/mol rotamer I − rotamer II
1	$n''_{O9} \rightarrow \pi^*_{C7O8}$	60.03	49.49	10.54
3	$n'_{O15} \rightarrow \sigma^*_{O9H12}$	18.57	20.19	−1.62
3	$n'_{O8} \rightarrow \sigma^*_{O14H13}$	14.06	19.23	−5.17
1	$n'_{O8} \rightarrow \sigma^*_{C1C7}$	12.73	16.80	−4.07
3	$n'_{O8} \rightarrow \sigma^*_{O14H13}$	10.44	9.07	1.37
2	$n''_{O8} \rightarrow \sigma^*_{O10H11}$	9.45	9.83	−0.38
3	$n'_{O15} \rightarrow \sigma^*_{O9H12}$	7.53	8.19	−0.66
2	$n'_{O8} \rightarrow \sigma^*_{O10H11}$	5.13	0	5.13

[a] Principal energy stabilization interactions (the more positive the $E(2)$ difference, the more stable) between the orbitals present on rotamers I, II of 2HBA that are responsible for one rotamer being more stable than the other. Stabilization energies were determined by the use of second-order perturbation theory.[12] $E(2)$ is the stabilization energy associated with delocalization. [b] Interaction types: 1 refers to intramolecular interactions, 2 refers to intramolecular hydrogen bonding interactions and 3 refers to intermolecular hydrogen bonding interactions.

TABLE 4: Primary Energy of Stabilization Interactions for 2HBA Monomer[a]

interaction type[b]	donor NBO (i) to acceptor NBO (j)	$E(2)$, kcal/mol rotamer I	$E(2)$, kcal/mol rotamer II	$E(2)$ difference, kcal/mol rotamer I − rotamer II
1	$n''_{O9} \rightarrow \pi^*_{C7O8}$	46.55	37.55	9.00
1	$n''_{O10} \rightarrow \pi^*_{C1C2}$	37.08	34.06	3.02
1	$n''_{O8} \rightarrow \sigma^*_{C1C7}$	13.12	17.25	−4.13
2	$n''_{O8} \rightarrow \sigma^*_{O10H11}$	13.72	8.80	4.92
2	$n''_{O8} \rightarrow \sigma^*_{O10H11}$	2.86	0.00	2.86

[a] Principal energy stabilization interactions (the more positive the $E(2)$ difference, the more stable) between the orbitals present on rotamers I, II of 2HBA that are responsible for one rotamer being more stable than the other. Stabilization energies were determined by the use of second-order perturbation theory.[12] $E(2)$ is the stabilization energy associated with delocalization. [b] Interaction types: 1 refers to intramolecular interactions and 2 refers to intramolecular hydrogen bonding interactions.

TABLE 5: Primary Energy of Stabilization Interactions for 2ABA Model Dimer[a]

interaction type[b]	donor NBO (i) to acceptor NBO (j)	$E(2)$, kcal/mol rotamer I	$E(2)$, kcal/mol rotamer II	$E(2)$ difference, kcal/mol rotamer I − rotamer II
1	$n''_{O9} \rightarrow \pi^*_{C7O8}$	56.66	51.14	5.52
1	$n_{N10} \rightarrow \pi^*_{C1C2}$	49.88	43.06	6.82
3	$n''_{O8} \rightarrow \sigma^*_{O14H13}$	20.77	21.86	−1.09
3	$n''_{O15} \rightarrow \sigma^*_{O9H12}$	16.59	17.86	−1.27
1	$n''_{O8} \rightarrow \sigma^*_{C1C7}$	12.96	16.38	−3.42
3	$n'_{O8} \rightarrow \sigma^*_{O14H13}$	9.36	9.49	−0.13
3	$n'_{O15} \rightarrow \sigma^*_{O9H12}$	6.74	7.31	−0.57
2	$n'_{O8} \rightarrow \sigma^*_{N10H11}$	2.90	0.00	2.90
2	$n''_{O8} \rightarrow \sigma^*_{N10H11}$	2.37	0.00	2.37
2	$n'_{O9} \rightarrow \sigma^*_{N10H11}$	0.00	4.06	−4.06

[a] Principal energy stabilization interactions (the more positive the $E(2)$ difference, the more stable) between the orbitals present on rotamers I, II of 2ABA that are responsible for one rotamer being more stable than the other. Stabilization energies were determined by the use of second-order perturbation theory.[12] $E(2)$ is the stabilization energy associated with delocalization. [b] Interaction types: 1 refers to intramolecular interactions, 2 refers to intramolecular hydrogen bonding interactions and 3 refers to intermolecular hydrogen bonding interactions.

TABLE 6: Primary Energy of Stabilization Interactions for 2ABA Monomer[a]

interaction type[b]	donor NBO (i) to acceptor NBO (j)	$E(2)$, kcal/mol rotamer I	$E(2)$, kcal/mol rotamer II	$E(2)$ difference, kcal/mol rotamer I − rotamer II
1	$n''_{O9} \rightarrow \pi^*_{C7O8}$	51.91	39.15	12.76
1	$n_{N10} \rightarrow \pi^*_{C1C2}$	50.06	39.75	10.31
1	$n''_{O8} \rightarrow \sigma^*_{C1C7}$	11.76	17.01	−5.25
2	$n''_{O8} \rightarrow \sigma^*_{N10H11}$	4.25	0.00	4.25
2	$n'_{O8} \rightarrow \sigma^*_{N10H11}$	1.67	0.00	1.67
2	$n'_{O9} \rightarrow \sigma^*_{N10H11}$	0.00	3.71	−3.71

[a] Principal energy stabilization interactions (the more positive the E(2) difference, the more stable) between the orbitals present on rotamers I, II of 2ABA that are responsible for one rotamer being more stable than the other. Stabilization energies were determined by the use of second-order perturbation theory.[12] $E(2)$ is the stabilization energy associated with delocalization. [b] Interaction types: 1 refers to intramolecular interactions and 2 refers to intramolecular hydrogen bonding interactions.

available from O9; in fact, the overlap integral is zero for the second set of lone pair electrons of O9. The net increase in stabilization for the 2HBA dimer is 4.75 and 7.78 kcal/mol for the monomer whereas the net increase in stabilization for the 2ABA dimer is 5.27 and 5.92 kcal/mol for the monomer.

Dimerization leads to increased stabilization relative to the isolated monomer, the differences in stabilization between rotamers I and II being most evident for 2HBA relative to 2ABA with both the 2-substituted benzoic acids paying a price in a decrease in intermolecular hydrogen bond stabilization in going from rotamer II to rotamer I, as can be seen from Tables 3 and 5. More specifically, the listed stabilization energies ($n'_{O8} \rightarrow \sigma^*_{O14H13}$, $n''_{O8} \rightarrow \sigma^*_{O14H13}$, $n'_{O15} \rightarrow \sigma^*_{O9H12}$ and $n''_{O15} \rightarrow \sigma^*_{O9H12}$) for intermolecular hydrogen bonding for rotamer I are 6.08 kcal/mol less stable for 2HBA and 3.06 kcal/mol less stable for 2ABA than for their respective rotamer II structures. For 2HBA, this loss in intermolecular hydrogen bonding stabilization is primarily a result of the decreased stabilization from the $n''_{O8} \rightarrow \sigma^*_{O14H13}$ interaction (5.17 kcal/mol). This decrease in n''_{O8} stabilization is offset by the increased participation of the intramolecular hydrogen bonding stabilization interaction $n'_{O8} \rightarrow \sigma^*_{O10H11}$ (5.13 kcal/mol), which occurs in rotamer I but not in rotamer II. For 2ABA, this loss in intermolecular hydrogen bonding stabilization is primarily a result of the decreased stabilization from both $n''_{O15} \rightarrow \sigma^*_{O9H12}$ (1.27 kcal/mol) and $n''_{O8} \rightarrow \sigma^*_{O14H13}$ (1.09 kcal/mol). This decrease in stabilization is offset by the increased participation of the intramolecular hydrogen bonding stabilization interaction $n'_{O8} \rightarrow \sigma^*_{N10H11}$ (2.90 kcal/mol) and $n''_{O8} \rightarrow \sigma^*_{N10H11}$ (2.37 kcal/mol), which occurs in rotamer I but not in rotamer II. That is, for both 2HBA and 2ABA there is a trade off between the increased stabilization afforded by the participation of O8 in the intramolecular hydrogen bond and a decrease in the intermolecular hydrogen bond stabilization when comparing rotamer I to rotamer II.

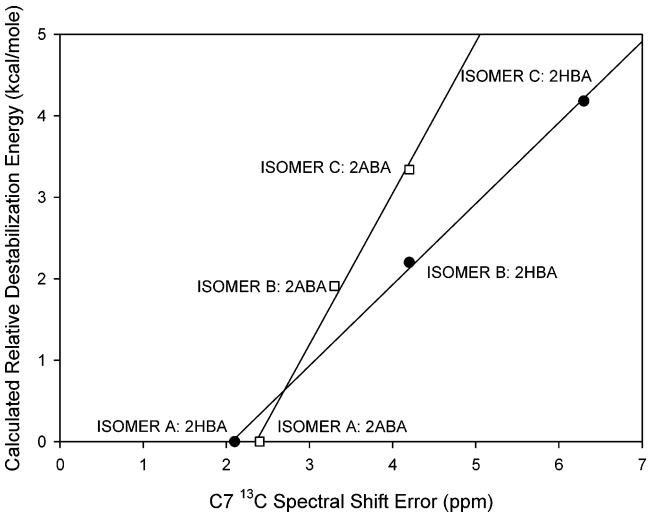

Figure 4. Plots of calculated relative energies of destabilization at the B3LYP/6-31+G(d)//B3LYP/6-31G level for 2HBA and 2ABA and the C7 ^{13}C spectral shift absolute value error. Correlation for 2HBA of $r^2 = 0.999$ (solid circle), correlation for 2ABA of $r^2 = 0.993$ (open square). The spectral shift errors are calculated by taking the absolute difference between the calculated model dimer rotamer spectral shift and the experimental spectral shift (see Table 2 C7 dimer |dif|). The calculated spectral shift errors for the B isomers (50% rotamer I and 50% rotamer II) were obtained by taking the average of the A (100% rotamer I) and C (100% rotamer II) isomer spectral shift errors.

Even though the complete isomers A, B and C given in Figure 3 could not be analyzed by DFT calculations, due to their size, one can still infer which isomer is preferred from the model dimer calculations. For both the monomeric and model dimer forms of 2HBA and 2ABA, the error in the carboxyl carbon's (C7) calculated ^{13}C chemical shift, when compared to the experimental ^{13}C chemical shift, is much greater for rotamer II than for rotamer I (see Tables 1 and 2) with rotamer II's calculated C7 ^{13}C spectral shift being smaller than rotamer I's. Thus, if either isomer B (contains 50% rotamer I and 50% rotamer II) or C (contains 100% rotamer II) occurred, the agreement with the overall carboxyl ^{13}C chemical shift would even be further from the observed experimental value, as compared to isomer A (100% rotamer I), because the experimental ^{13}C chemical shift represents a weighted average of the species present in solution. In addition, as can be seen from Figure 4, the optimized structures obtained for the full dimers at B3LYP/6-31G followed by single point energy calculations at B3LYP/6-31+G(d) exhibit an energetic preference for the same isomer that is indicated by the NMR results obtained from the higher basis set calculations on the model dimer systems.

The preference of rotamer I over rotamer II, the predilection for isomer A, the planar intermolecular hydrogen bonded dimers,

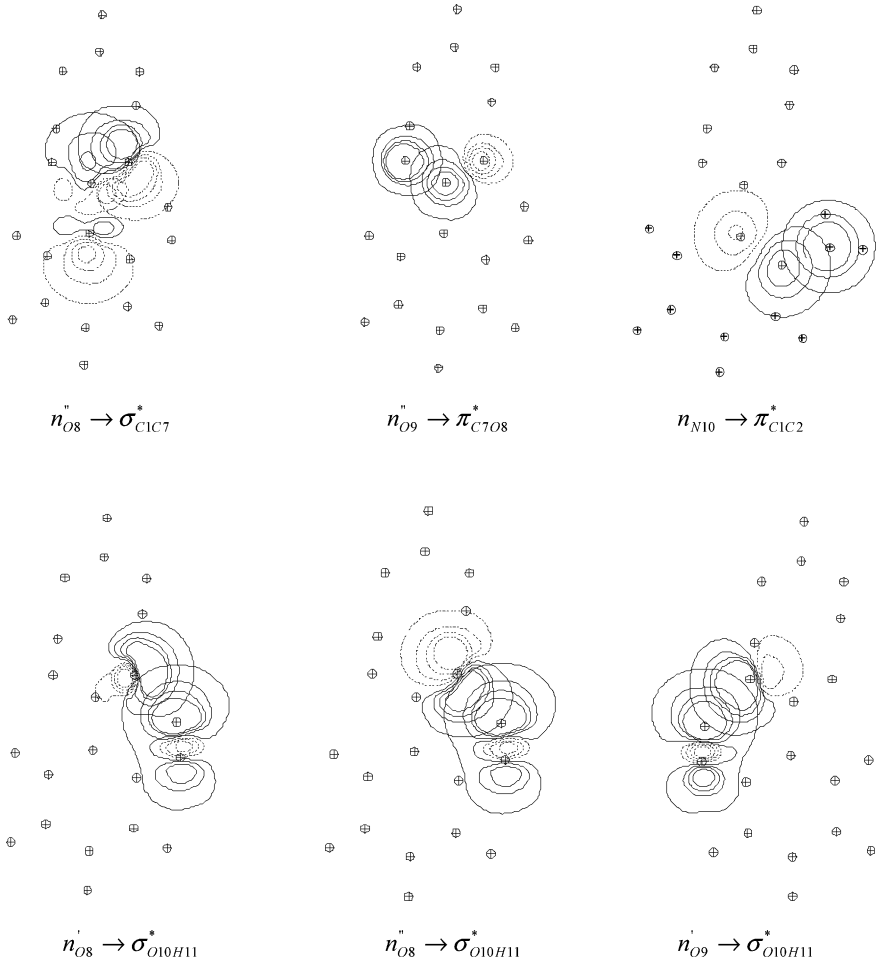

Figure 5. Representative intramolecular orbital interactions for entries of Tables 3 and 5, all leading to significant differences in stabilizations between rotamers I and II. Solid contour lines represent the positive phase and dotted contour lines represent the negative phase.

and the intramolecular hydrogen bonding predicted by the gas phase calculation in conjunction with experimental solution NMR ^{13}C chemical shift data are entirely consistent with crystal structures obtained for 2HBA[24−26] and 2ABA.[27−29] For 2HBA, the comparison between the critical bond lengths, bond angles and dihedral angles gives average differences of -0.009 ± 0.016 Å, $-0.047 \pm 0.656°$, and $+0.487 \pm 0.862°$, respectively, and for 2ABA, $+0.012 \pm 0.007$ Å, $-0.054 \pm 0.662°$, and $+1.380 \pm 0.682°$, respectively. (See Supporting Information for details.) This suggests not only that the gas phase calculations are consistent with crystal structures but also that the model dimers provide an accurate assessment of the full dimer crystal structure.

Further emphasis of the importance of the intramolecular hydrogen bond in determining the type of intermolecular interactions observed can be seen from examination of the crystal structure of 3-hydroxybenzoic acid.[30] For 3-hydroxybenzoic acid, an intramolecular hydrogen bond is unable to form. However, the hydroxyl group in the 3-position is now found to participate in intermolecular hydrogen bonds with another 3-hydroxylbenzoic acid molecule either with its 3-hydroxyl group or with its carboxylic acid moiety, leading to markedly different polymorphs in the crystal phase.[30] In summary, the close agreement between the gas phase and crystal structures is a rather unusual finding. Generally, subtle differences in crystal lattice forces, crystal lattice packing constraints, entropic changes, kinetic factors and preorganization of the molecules prior to nucleation all can result in markedly different crystal structures.[31,32] It appears then that the strong cyclic dimer forming intermolecular hydrogen bonds, the innate steric bulk of the attached benzene ring, the efficient crystal packing of the planar cyclic dimer structures, and the presence of intramolecular hydrogen bonds, are sufficient to allow the determined gas phase structure to persist in the crystal lattice.[33]

From Tables7 and 8, the major contribution in bringing the calculated C7 carboxylic ^{13}C chemical shift, which is in part anisotropic in nature, into closer agreement with the experimental chemical shift is that of a non-Lewis induced (field-dependent) effect of n''_{O8} on C7. This interaction contributes a 4.95 and 8.41 ppm improvement in C7's ^{13}C chemical shift for the 2HBA model dimer and monomer, and a 4.12 and 2.53 ppm improvement for the 2ABA model dimer and monomer. In particular, this involves primarily non-Lewis induced differences due to the $n''_{O8} \rightarrow \sigma^*_{C1C7}$ and $n''_{O8} \rightarrow \sigma^*_{C7O9}$ interactions present in the 2HBA and 2ABA monomers and model dimers. All these interactions favor rotamer I over rotamer II in terms of an improved agreement between the calculated and experimental C7 ^{13}C chemical shift. That is, the calculated ^{13}C chemical shifts are always less positive than experimental ^{13}C chemical shifts (see Tables 1 and 2 for C7's experimental and calculated ^{13}C chemical shifts). Because the differences between rotamer I and rotamer II are always positive (see Tables 7 and 8), this implies that rotamer I is always more positive and as such closer to the experimental C7 ^{13}C chemical shift.

Summary

Determination of the preferential molecular rotamer and isomer is obtained if the monomers and model dimers are

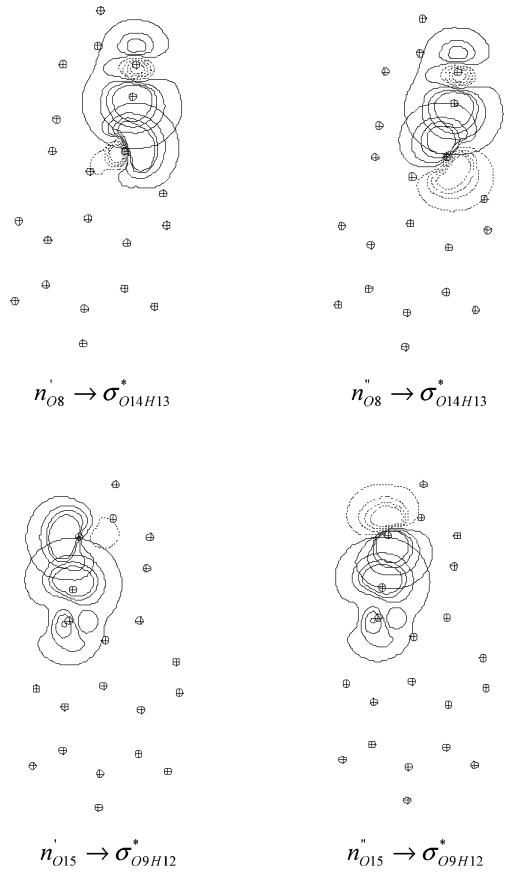

Figure 6. Similar to Figure 5, for representative intermolecular orbital interactions of Tables 3 and 5.

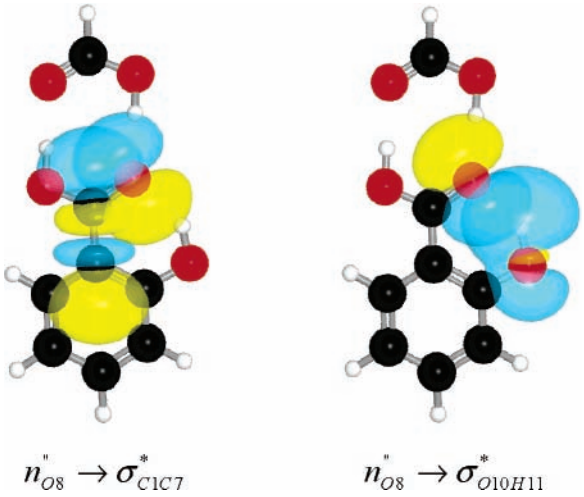

Figure 7. Illustration of how the p-type oxygen lone pair can hyperconjugate with both the σ^*_{C1C7} and σ^*_{O10H11} orbitals.

analyzed either by finding the structure with the best agreement between calculated and experimental ^{13}C chemical shifts or by obtaining the lowest energy structure. NMR data indicate the presence of dimerization as shown by a marked improvement in agreement between experimental and theoretical C7 ^{13}C chemical shift data when the dimer model is used. Thus, the carboxylic carbon ^{13}C chemical shift provides a powerful diagnostic probe for the determination of molecular conformation of 2HBA and 2ABA. The dimers are stabilized by resonance assisted intermolecular hydrogen bonds and additionally by intramolecular hydrogen bonds. Energy of stabilization trade offs are made, resulting in the lowest energy isomer giving

TABLE 7: Principal Orbital Interactions Responsible for the Improved Agreement in the C7 Calculated and Experimental ^{13}C Chemical Shift for 2HBA[a]

	C7/n''_{O8} (ppm)	$n''_{O8} \rightarrow \sigma^*_{C1C7}$ (ppm)	$n''_{O8} \rightarrow \sigma^*_{C7O9}$ (ppm)
		model dimer	
		rotamer I	
L	9.93 (11.37)		
NL	−20.86 (−18.25)	−9.88 (−9.35)	−14.25 (−13.08)
		rotamer II	
L	11.53 (13.22)		
NL	−27.42 (−22.93)	−13.28 (−12.59)	−16.88 (−15.03)
		rotamer I − rotamer II	
L	−1.61 (−1.85)		
NL	6.56 (4.68)	3.40 (3.24)	2.63 (1.95)
L+NL[b]	4.95 (2.83)		
		monomer	
		rotamer I	
L	11.44 (12.16)		
NL	−19.12 (−19.70)	−3.83 (−4.29)	−22.25 (−21.46)
		rotamer II	
L	10.58 (12.50)		
NL	−26.68 (−25.82)	−6.13 (−6.62)	−25.34 (−23.71)
		rotamer I − rotamer II	
L	0.85 (−0.33)		
NL	7.56 (6.13)	2.30 (2.33)	3.10 (2.24)
L+NL[b]	8.41 (5.79)		

[a] Isotropic shielding values are given where L refers to Lewis and NL refers to non-Lewis. The terms in parentheses are the induced (field-dependent) component. The difference between the no parentheses values and the parentheses values gives the unperturbed (field-free) component. The unperturbed and induced GIAO contributions given here are parallel to the diamagnetic and paramagnetic terms in Ramsey's non-GIAO theory. Columns 3 and 4 give the most important donor acceptor contributors to n''_{O8}'s overall effect on C7, which is given in column 2. [b] L+NL is the overall improvement in ppm for the n''_{O8} affect on C7's ^{13}C chemical shift. In all cases, the ab initio shielding values have been converted to ppm by multiplying by −0.8710 obtained from the Figure 1 regression equation.

up some of its intermolecular hydrogen bond's stabilization for an increase in its intramolecular hydrogen bond stabilization. The intermolecular hydrogen bond stabilization of the dimer is occurring primarily due to $n_O \rightarrow \sigma^*_{OH}$ interactions. The subtleties leading to the preference of rotamer I, whether considering the monomers or the model dimers, reveal increased stabilization, resulting principally from the $n''_{O9} \rightarrow \pi^*_{C7O8}$ interaction. Also, preferential intramolecular hydrogen bond stabilization of rotamer I relative to rotamer II is the result of an additional $n_{O8} \rightarrow \sigma^*_{O10H11}$ interaction in 2HBA and additional $n_{O8} \rightarrow \sigma^*_{N10H11}$ interactions in 2ABA. Prediction of the preferential isomers, based on C7 ^{13}C chemical shifts of model dimers, and their strong correlation to those obtained by single point energy calculations on the dimer, demonstrate the potential utility of using model systems to characterize computationally inaccessible larger systems. Crystal structures are also consistent with the insights acquired from gas phase model dimer calculations and ^{13}C chemical shift measurements. The key chemical shift differences can be traced to anisotropic non-Lewis field-dependent differences in the $n''_{O8} \rightarrow \sigma^*_{C1C7}$ and $n''_{O8} \rightarrow \sigma^*_{C7O9}$ interactions. Finally, orbital interaction analysis, whether in terms of the contributions to energy of stabilization or ^{13}C chemical shift contributions, reveals that the conclusions drawn for these substituted benzoic acid derivatives, whether viewed as monomers or model dimers, yield highly transferable results when interpreted in terms of an NBO analysis.

TABLE 8: Principal Orbital Interactions Responsible for the Improved Agreement in the C7 Calculated and Experimental ^{13}C Chemical Shift for 2ABA[a]

	C7/n''_{O8} (ppm)	$n''_{O8} \rightarrow \sigma^*_{C1C7}$ (ppm)	$n''_{O8} \rightarrow \sigma^*_{C7O9}$ (ppm)
		model dimer	
		rotamer I	
L	9.49 (11.45)		
NL	−19.21 (−16.49)	−11.72 (−10.89)	−13.26 (−11.90)
		rotamer II	
L	10.63 (12.34)		
NL	−24.47 (−20.91)	−12.26 (−11.79)	−15.16 (−13.58)
		rotamer I − rotamer II	
L	−1.15 (−0.89)		
NL	5.26 (4.42)	0.54 (0.90)	1.90 (1.69)
L+NL[b]	4.12 (3.53)		
		monomer	
		rotamer I	
L	8.89 (10.42)		
NL	−21.58 (−20.96)	1.72 (2.00)	−22.18 (−20.91)
		rotamer II	
L	9.59 (11.55)		
NL	−24.81 (−24.51)		−24.64 (−23.02)
		rotamer I − rotamer II	
L	−0.71 (−1.14)		
NL	3.23 (3.55)	1.72 (2.00)	2.46 (2.11)
L+NL[b]	2.53 (2.41)		

[a] Isotropic shielding values are given where L refers to Lewis and NL refers to non-Lewis. The terms in parentheses are the induced (field-dependent) component. The difference between the no parentheses values and the parentheses values gives the unperturbed (field-free) component. The unperturbed and induced GIAO contributions given here are parallel to the diamagnetic and paramagnetic terms in Ramsey's non-GIAO theory. Columns 3 and 4 give the most important donor acceptor contributors to n''_{O8}'s overall effect on C7, which is given in column 2. [b] L+NL is the overall improvement in ppm for the n''_{O8} affect on C7's ^{13}C chemical shift. In all cases, the ab initio shielding values have been converted to ppm by multiplying by −0.8710 obtained from the Figure 1 regression equation.

Acknowledgment. NMR spectra were obtained at the UW Biochemistry NMRFAM and at the UW School of Pharmacy's Analytical Instrumentation Center. We also acknowledge helpful discussions with Professors Lian Yu, Kenneth Connors, George Zografi and Dr. Thomas Stringfellow of the School of Pharmacy, as well as Dr. Ilia Guzei in the Department of Chemistry at UW Madison.

Supporting Information Available: Tables of bond lengths and angles, bond orders, and charges. This material is available free of charge via the Internet at http://pubs.acs.org.

References and Notes

(1) Forsyth, D. A.; Sebag, A. B. *J. Am. Chem. Soc.* **1997**, *119*, 9483.
(2) Abraham, R. J. F., J.; Loftus, P. *Introduction to NMR Spectroscopy*; John Wiley & Sons: New York, 1988.
(3) Koehorst, R. B. M.; Spruijt, R. B.; Vergeldt, F. J.; Hemminga, M. A. *Biophys. J.* **2004**, *87*, 1445.
(4) Rezai, T.; Yu, B.; Millhauser, G. L.; Jacobson, M. P.; Lokey, R. S. *J. Am. Chem. Soc.* **2006**, *128*, 2510.
(5) Chesnut, D. B. *Rev. Comput. Chem.* **1996**, *8*, 245.
(6) Cheeseman, J. R.; Trucks, G. W.; Keith, T. A.; Frisch, M. J. *J. Chem. Phys.* **1996**, *104*, 5497.
(7) Glendening, E. D.; Feller D. *J. Am. Chem. Soc.* **1996**, *118*, 6052.
(8) Friebolin, H. *Basic One- and Two-Dimensional NMR Spectroscopy*, 3rd revised ed.; Wiley-VCH: New York, 1998.
(9) Bohmann, J. A.; Weinhold, F.; Farrar, T. C. *J. Chem. Phys.* **1997**, *107*, 1173.
(10) Frisch, M. J.; Trucks, G. W.; Schlegal, H. B.; Scuseria, G. E.; Robb, M. A.; Chessman, J. R.; Zakrzewski, V. G.; Montgomery, J. A.; Stratmann, R. E.; Burant, J. C.; Dapparich, S.; Millam, J. M.; Daneils, A. D.; Kudin, K. N.; Strain, M. C.; Farkas, O.; Tomasi, J.; Barone, V.; Cossi, M.; Cammi, R.; Mennucci, B.; Pomelli, C.; Adamo, C.; Clifford, S.; Ochterski, J.; Petersson, G. A.; Ayala, P. Y.; Cui, Q.; Morokuma, K.; Malick, D. K.; Rabuck, A. D.; Raghavachari, K.; Foresman, J. B.; Cioslowski, J.; Ortiz, J. B.; Stefanov, B. B.; Lui, G.; Liashenko, A.; Piskorz, P.; Komaromi, A.; Gomperts, R.; Martin, R. L.; Fox, D. J.; Keith, T.; Al-Laham, A.; Peng, C. Y.; Nanayakkara, M. W.; Gonzalez, C.; Challacombe, M.; Gill, P. M. W.; Johnson, B. G.; Chen, W.; Wong, M. W.; Andres, J. L.; Head-Gordon, M.; Replogle, E. S.; Pople, J. A. *Gaussian 98*; Gaussian, Inc.: Pittsburgh, PA, 1998.
(11) Levine, I. N. *Quantum Chemistry*, 5th ed.; Prentice Hall: Upper Saddle River, NJ, 2000.
(12) de Dios, A. C. *Prog. Nucl. Magn. Reson. Spectrosc.* **1996**, *29*, 229.
(13) Weinhold, F. A. Natural Bond Orbital Methods. In *Encyclopedia of Computational Chemistry*; John Wiley: Chichester, U.K., 1998; Vol. 3, p 1792.
(14) Braun, S.; Kalinowski, H.-O.; Berger, S. *150 and More Basic NMR Experiments*, 2nd expanded ed.; Wiley-VCH: New York, 1998.
(15) Kopacz, S.; Kalembkiewicz, J.; Szantula, J. *Zh. Obshch. Khim.* **1984**, *54*, 721.
(16) Titan; 1.05 ed.; Wavefunction, Inc./Schrodinger, Inc.: Irvine, 1999.
(17) Glendening, E. D.; Badenhoop, J. K.; Reed, A. E.; Carpenter, J. E.; Bohmann, J. A.; Weinhold, F. NBO 5.0; Theoretical Chemistry Institute, University of Wisconsin, Madison, WI, 2001 (www.chem.wisc.edu/~nbo5).
(18) Wendt, M.; Weinhold, F. NBOView: NBO Orbital Graphics; 1.0 ed., 2001.
(19) Allen, G.; Caldin, E. F. *Q. Rev. (London)* **1953**, *7*, 255.
(20) Wall, F. T.; Rouse, P. E., Jr. *J. Am. Chem. Soc.* **1941**, *63*, 3002.
(21) Strong, L. E.; Brummel, C. L.; Ryther, R.; Radford, J. R.; Pethybridge, A. D. *J. Solution Chem.* **1988**, *17*, 1145.
(22) Gilli, G.; Bellucci, F.; Ferretti, V.; Bertolasi, V. *J. Am. Chem. Soc.* **1989**, *111*, 1023.
(23) Gilli, P.; Ferretti, V.; Bertolasi, V.; Gilli, G. *Adv. Mol. Struct. Res.* **1996**, *2*, 67.
(24) Cochran, W. *Acta Crystallogr.* **1953**, *6*, 260.
(25) Sundaralingam, M.; Jensen, L. H. *Acta Crystallogr.* **1965**, *18*, 1053.
(26) Bacon, G. E.; Jude, R. J. *Z. Kristallogr., Kristallgeom., Kristallphys., Kristallchem.* **1973**, *138*, 19.
(27) Boone, C. D. G.; Derissen, J. L.; Schoone, J. C. *Acta Crystallogr., Sect. B: Struct. Crystallogr. Cryst. Chem.* **1977**, *B33*, 3205.
(28) Hardy, G. E.; Kaska, W. C.; Chandra, B. P.; Zink, J. I. *J. Am. Chem. Soc.* **1981**, *103*, 1074.
(29) Takazawa, H.; Ohba, S.; Saito, Y. *Acta Crystallogr., Sect. C: Cryst. Struct. Commun.* **1986**, *C42*, 1880.
(30) Gridunova, G. V.; Furmanova, N. G.; Struchkov, Y. T.; Ezhkova, Z. I.; Grigor'eva, L. P.; Chayanov, B. A. *Kristallografiya* **1982**, *27*, 267.
(31) Sarma, J. A. R. P.; Desiraju, G. R. *Cryst. Growth & Design* **2002**, *2*, 93.
(32) Gavezzotti, A. *Acc. Chem. Res.* **1994**, *27*, 309.
(33) Beyer, T.; Price, S. L. *J. Phys. Chem. B* **2000**, *104*, 2647.